Sources of Seismic Waves

- Impact
- Volcanic
- Landslide
- Explosion
  - Buried or surface
- Harmonic Tremor
  - Unsteady fluid flow
- Continuous Excitation
  - Wind, microseism, couple ocean/atmosphere (hum)
- Earthquakes

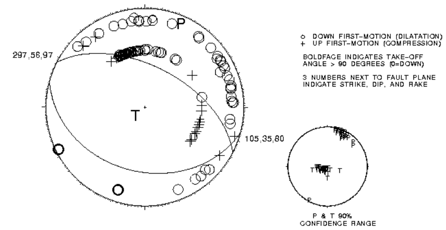

Types of Seismograms

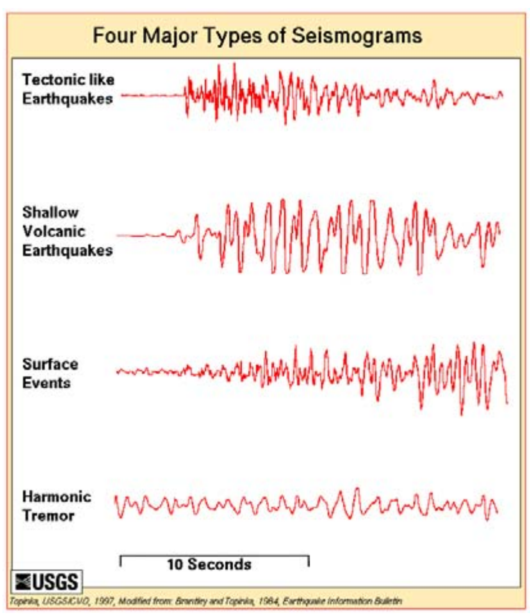

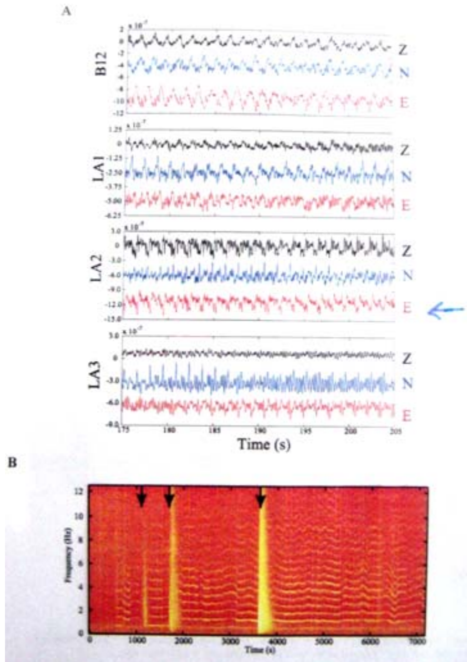

Volcanic Tremor

Seismic excitation from unsteady fluid flow

Courtesy of Peggy Hellweg (BSL)

Volcanic Earthquakes & Explosions

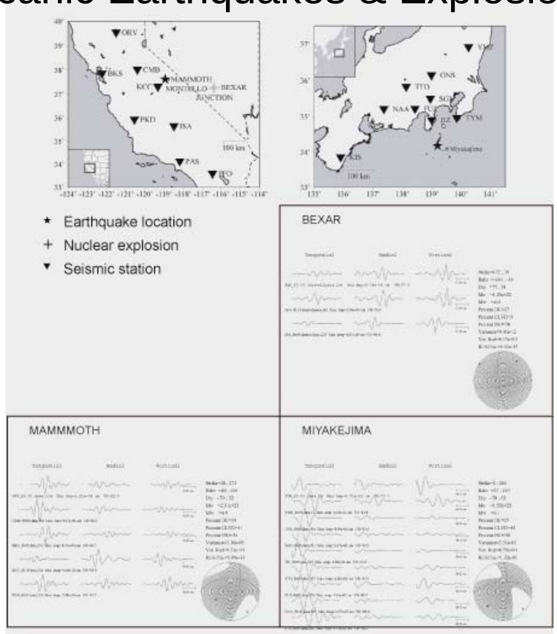

Yosemite Rock Fall

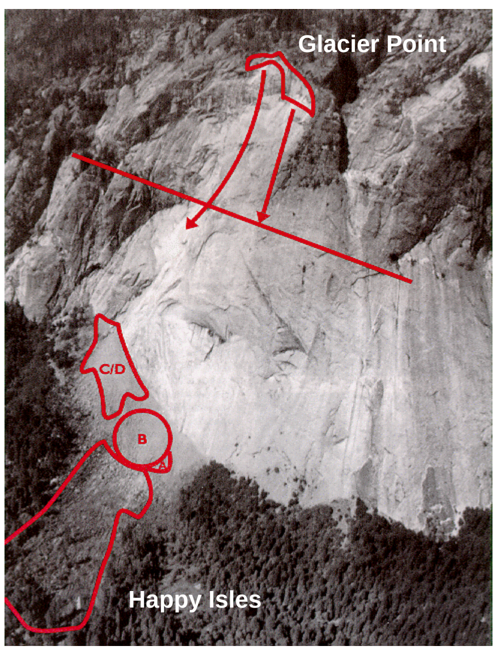

80,000 ton
(72.5 MKg)

Yosemite Rock Fall

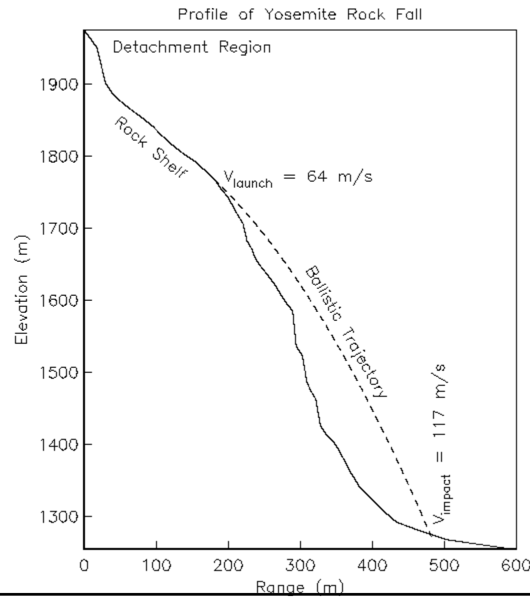

Transverse velocity is 78 m/s (174mph)

Debris filled wind blast

Yosemite Rock Fall

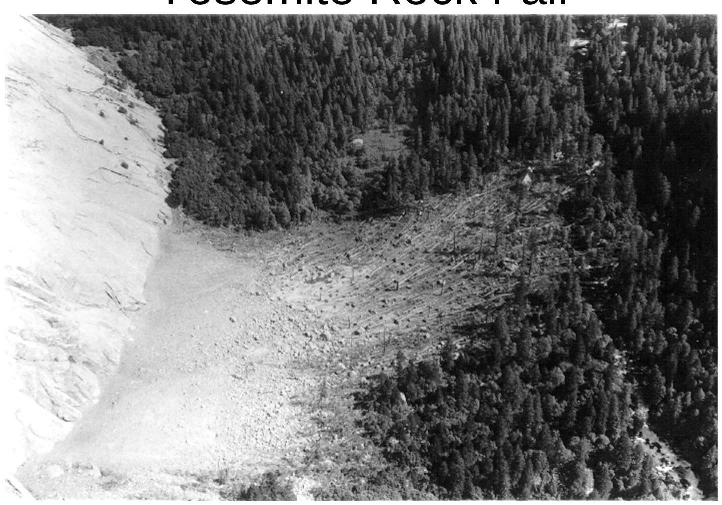

Yosemite Rock Fall

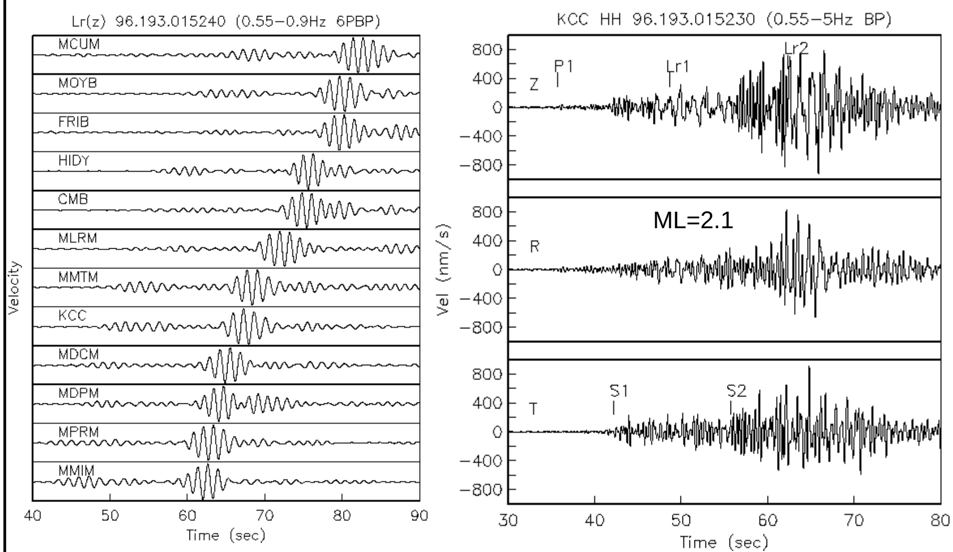

http://seismo.berkeley.edu/seismo/events_of_interest/yosemite/eoi_yos.html

Kalapana Earthquake??

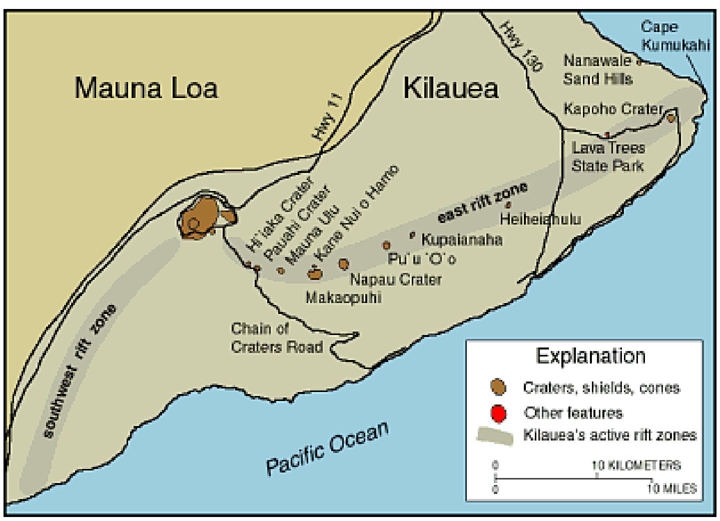

Material from:
http://hvo.wr.usgs.gov/earthquakes/destruct/1975Nov29/

Kalapana Earthquake??

Land subsidence of 12 ft

Tsunami runup 47 ft

Two deaths & $4.1 million in damage

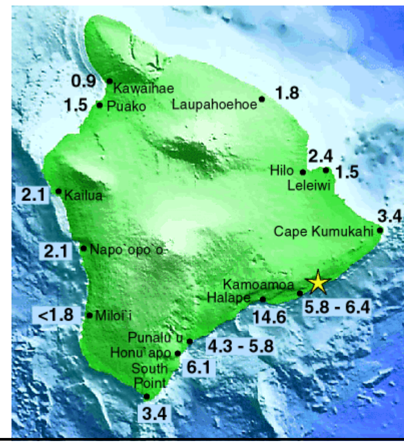

Kalapana Earthquake??

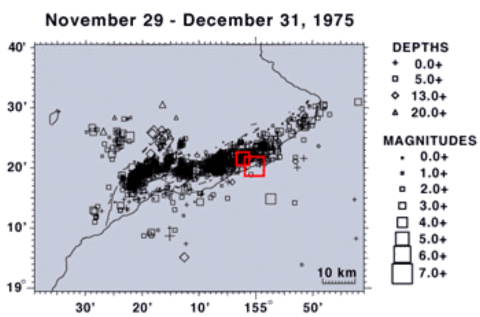

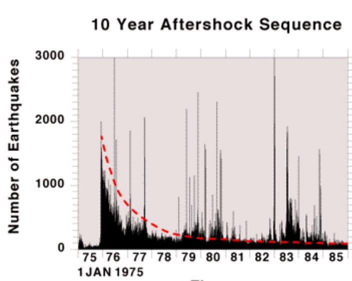

Kalapana Earthquake??

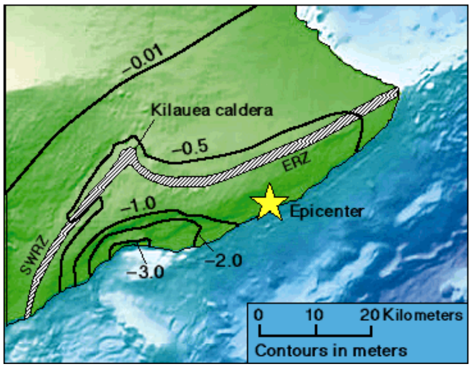

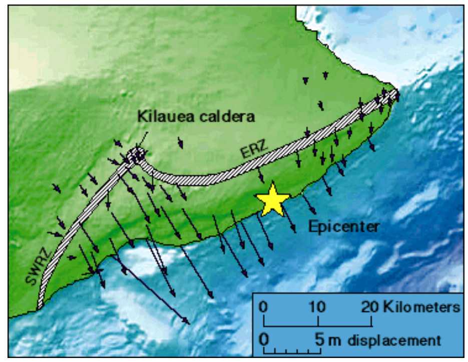

Geodetic data are consistent with a slump

Kalapana Earthquake??

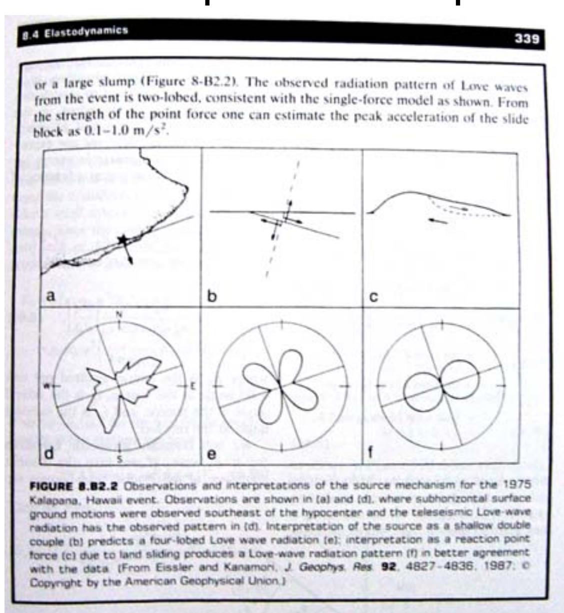

8.4 Elastodynamics 339

or a large slump (Figure 8-B2.2). The observed radiation pattern of Love waves from the event is two-lobed, consistent with the single-force model as shown. From the strength of the point force one can estimate the peak acceleration of the slide block as 0.1–1.0 m/s^2.

FIGURE 8.B2.2 Observations and interpretations of the source mechanism for the 1975 Kalapana, Hawaii event. Observations are shown in (a) and (d), where subhorizontal surface ground motions were observed southeast of the hypocenter and the teleseismic Love-wave radiation has the observed pattern in (d). Interpretation of the source as a shallow double couple (b) predicts a four-lobed Love wave radiation (e); interpretation as a reaction point force (c) due to land sliding produces a Love-wave radiation pattern (f) in better agreement with the data. (From Eissler and Kanamori, *J. Geophys. Res.* **92**, 4827–4836, 1987; © Copyright by the American Geophysical Union.)

Kalapana Earthquake??

424 M. Nettles and G. Ekström

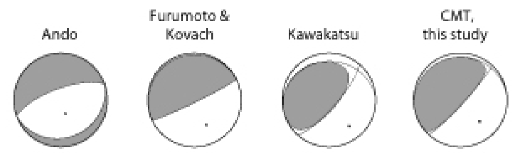

mechanism:	first motions	first motions	CMT analysis	CMT analysis
moment:	1.8e20 N-m	1.2e20 N-m	1.4e20 N-m	3.8e20 N-m
	100-s s. w.	P, S, 100-s s. w.	200 –250-s s.w.	>200-s s.w.

Figure 2. Comparison of teleseismically determined focal mechanisms for the Kalapana earthquake. The method by which the focal mechanisms were determined is listed to the right of the heading "mechanism"; the scalar moment determined in each study is listed to the right of the heading "moment." The data set used to determine the moment is also indicated (e.g., "100-s s.w."= 100-sec surface waves). The focal mechanisms are from (left to right) Ando (1979), Furumoto and Kovach (1979), Kawakatsu (1989), and this study. Ando (1979) used crustal deformation data and surface-wave radiation patterns to help constrain the focal mechanism he determined from the P-wave radiation pattern.

Kalapana Earthquake??

426 M. Nettles and G. Ekström

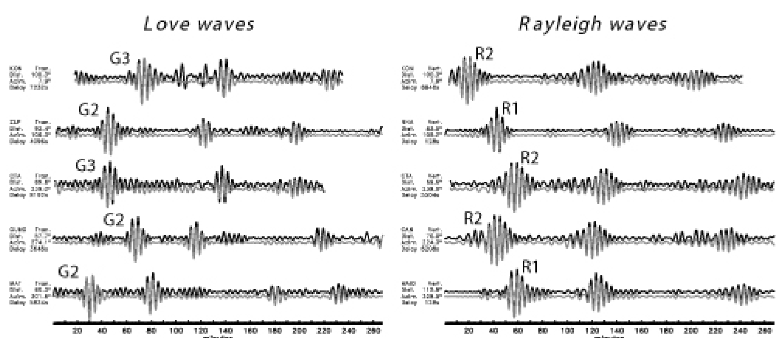

Figure 3. Examples of the fit to Love and Rayleigh waves (vertical component is shown) achieved in this study. Data seismograms are shown in black and synthetic seismograms in gray. The synthetic seismograms are offset slightly from the data for clarity. The distance and azimuth to the earthquake epicenter are indicated for each station. "Delay" gives the time of the first sample of each seismogram with respect to the origin time of the earthquake. The timescale refers to the start time of each record shown. The first wave group in each trace has been labeled.

Kalapana Earthquake??

Long-Period Source Characteristics of the 1975 Kalapana, Hawaii, Earthquake 427

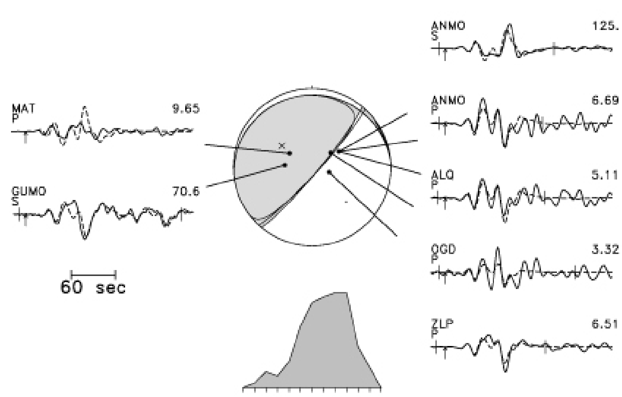

Figure 4. Results of body-wave analysis of the Kalapana earthquake. Long-period data seismograms are shown as solid lines; the calculated synthetic seismograms are shown as dashed lines. The wave type (P or S) is given below the name of each station. The maximum amplitude (in microns) for each trace is shown at right of each seismogram. Short vertical bars show the time window included for each station; where the bars are missing (MAT), the seismogram was not included in the inversion. The arrows show the arrival times of the P and S waves, as explained in the text. Shaded focal mechanism is that determined by inversion of the long-period body waves; the focal mechanism shown in outline only is that from the GMT inversion. The retrieved source time function is shown at the bottom of the plot. The depth of the earthquake was held fixed at 10 km in this inversion.

Non Volcanic Seismic Tremor & Aseismic Subduction Slip

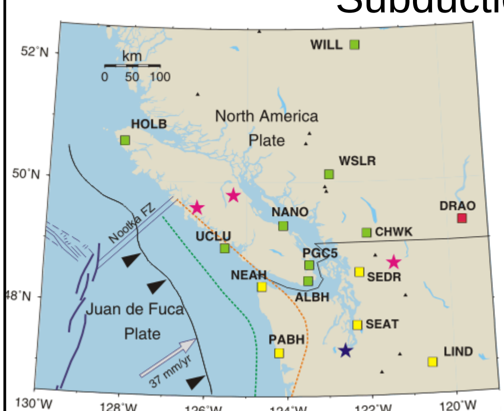

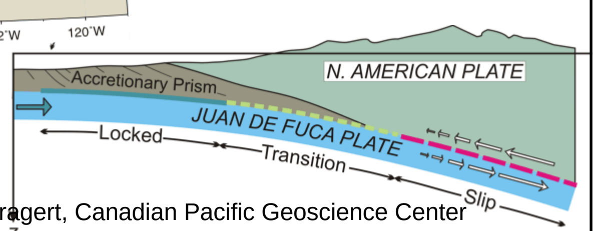

Gary Rodgers & Herb Dragert, Canadian Pacific Geoscience Center

Non Volcanic Seismic Tremor & Aseismic Subduction Slip

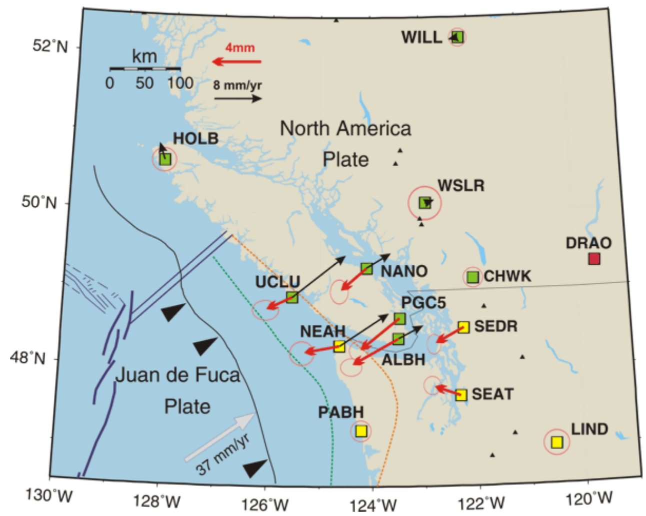

Gary Rodgers & Herb Dragert, Canadian Pacific Geoscience Center

Non Volcanic Seismic Tremor & Aseismic Subduction Slip

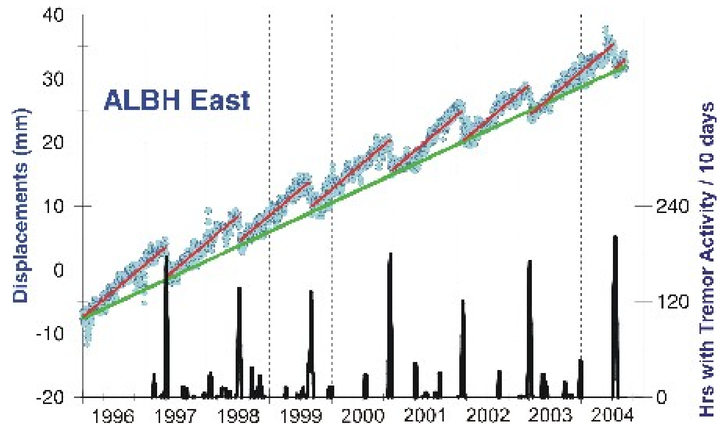

Gary Rodgers & Herb Dragert, Canadian Pacific Geoscience Center

Non Volcanic Seismic Tremor & Aseismic Subduction Slip

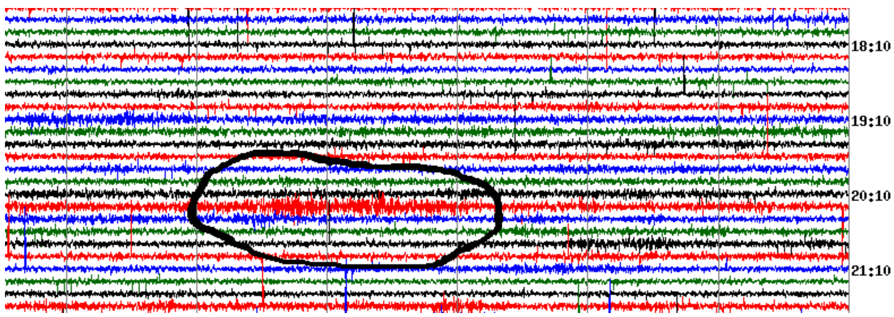

Gary Rodgers & Herb Dragert, Canadian Pacific Geoscience Center

Non Volcanic Seismic Tremor & Aseismic Subduction Slip

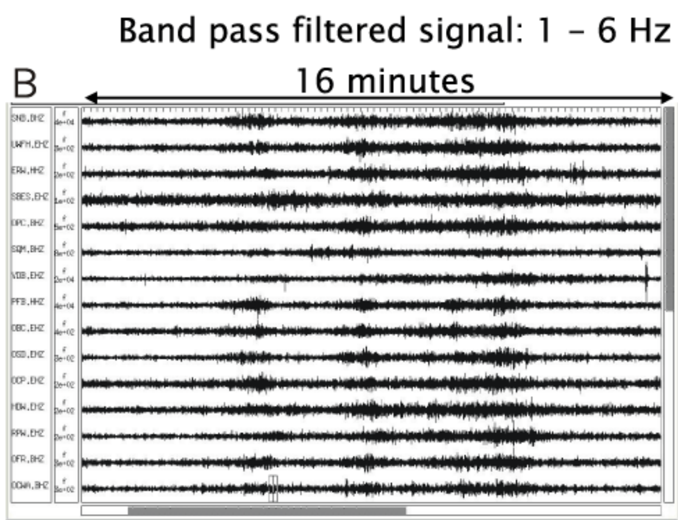

Gary Rodgers & Herb Dragert, Canadian Pacific Geoscience Center

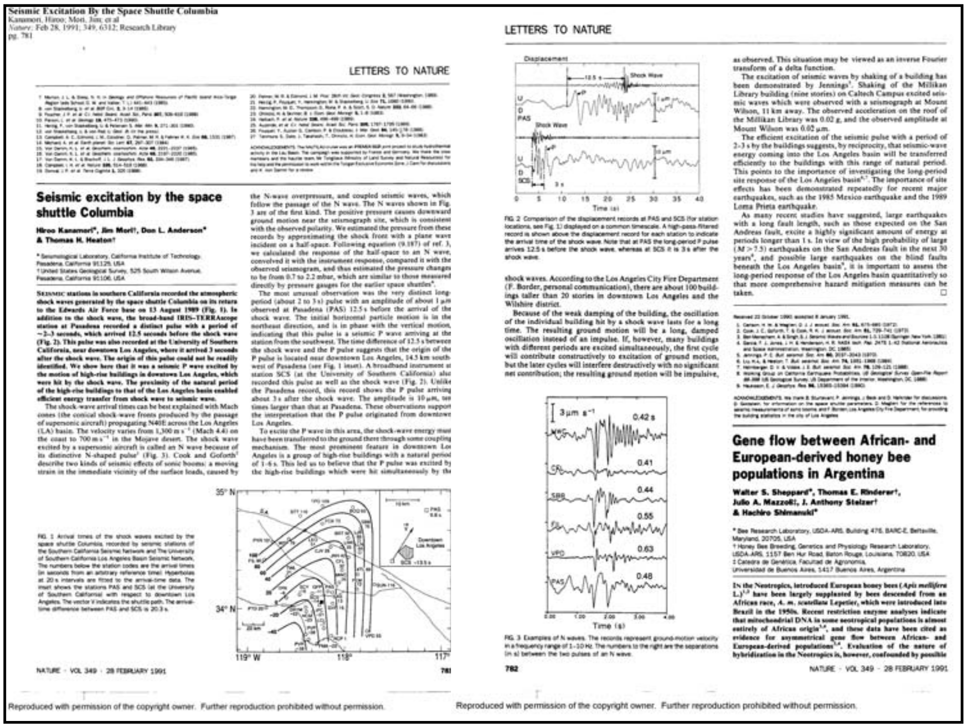

Seismic Excitation By the Space Shuttle Columbia
Kanamori, Hiroo; Mori, Jim; et al
Nature; Feb 28, 1991; 349, 6312; Research Library
pg. 781

Seismic excitation by the space shuttle Columbia

Hiroo Kanamori*, Jim Mori†, Don L. Anderson* & Thomas H. Heaton†

* Seismological Laboratory, California Institute of Technology, Pasadena, California 91125, USA
† United States Geological Survey, 525 South Wilson Avenue, Pasadena, California 91106, USA

SEISMIC stations in southern California recorded the atmospheric shock waves generated by the space shuttle Columbia on its return to the Edwards Air Force base on 13 August 1989 (Fig. 1). In addition to the shock wave, the broad-band IRIS–TERRAscope station at Pasadena recorded a distinct pulse with a period of ~2–3 seconds, which arrived 12.5 seconds before the shock wave (Fig. 2). This pulse was also recorded at the University of Southern California, near downtown Los Angeles, where it arrived 3 seconds after the shock wave. The origin of this pulse could not be readily identified. We show here that it was a seismic P wave excited by the motion of high-rise buildings in downtown Los Angeles, which were hit by the shock wave. The proximity of the natural period of the high-rise buildings to that of the Los Angeles basin enabled efficient energy transfer from shock wave to seismic wave.

The shock-wave arrival times can be best explained with Mach cones (the conical shock-wave fronts produced by the passage of supersonic aircraft) propagating N40E across the Los Angeles (LA) basin. The velocity varies from 1,300 m s^{-1} (Mach 4.4) on the coast to 700 m s^{-1} in the Mojave desert. The shock wave excited by a supersonic aircraft is called an N wave because of its distinctive N-shaped pulse[1] (Fig. 3). Cook and Goforth[2] describe two kinds of seismic effects of sonic booms: a moving strain in the immediate vicinity of the surface loads, caused by the N-wave overpressure, and coupled seismic waves, which follow the passage of the N wave. The N waves shown in Fig. 3 are of the first kind. The positive pressure causes downward ground motion near the seismograph site, which is consistent with the observed polarity. We estimated the pressure from these records by approximating the shock front with a plane wave incident on a half-space. Following equation (9.187) of ref. 3, we calculated the response of the half-space to an N wave, convolved it with the instrument response, compared it with the observed seismogram, and thus estimated the pressure changes to be from 0.7 to 2.2 mbar, which are similar to those measured directly by pressure gauges for the earlier space shuttles[4].

The most unusual observation was the very distinct long-period (about 2 to 3 s) pulse with an amplitude of about 1 μm observed at Pasadena (PAS) 12.5 s before the arrival of the shock wave. The initial horizontal particle motion is in the northeast direction, and is in phase with the vertical motion, indicating that this pulse is a seismic P wave arriving at the station from the southwest. The time difference of 12.5 s between the shock wave and the P pulse suggests that the origin of the P pulse is located near downtown Los Angeles, 14.5 km south-west of Pasadena (see Fig. 1 inset). A broadband instrument at station SCS (at the University of Southern California) also recorded this pulse as well as the shock wave (Fig. 2). Unlike the Pasadena record, this record shows the P pulse arriving about 3 s after the shock wave. The amplitude is 10 μm, ten times larger than that at Pasadena. These observations support the interpretation that the P pulse originated from downtown Los Angeles.

To excite the P wave in this area, the shock-wave energy must have been transferred to the ground there through some coupling mechanism. The most prominent feature in downtown Los Angeles is a group of high-rise buildings with a natural period of 1–6 s. This led us to believe that the P pulse was excited by the high-rise buildings which were hit simultaneously by the shock waves. According to the Los Angeles City Fire Department (F. Border, personal communication), there are about 100 buildings taller than 20 stories in downtown Los Angeles and the Wilshire district.

Because of the weak damping of the building, the oscillation of the individual building hit by a shock wave lasts for a long time. The resulting ground motion will be a long, damped oscillation instead of an impulse. If, however, many buildings with different periods are excited simultaneously, the first cycle will contribute constructively to excitation of ground motion, but the later cycles will interfere destructively with no significant net contribution; the resulting ground motion will be impulsive, as observed. This situation may be viewed as an inverse Fourier transform of a delta function.

The excitation of seismic waves by shaking of a building has been demonstrated by Jennings[5]. Shaking of the Millikan Library building (nine stories) on Caltech Campus excited seismic waves which were observed with a seismograph at Mount Wilson, 11 km away. The observed acceleration on the roof of the Millikan Library was 0.02 g, and the observed amplitude at Mount Wilson was 0.02 μm.

The efficient excitation of the seismic pulse with a period of 2–3 s by the buildings suggests, by reciprocity, that seismic-wave energy coming into the Los Angeles basin will be transferred efficiently to the buildings with this range of natural period. This points to the importance of investigating the long-period site response of the Los Angeles basin[6,7]. The importance of site effects has been demonstrated repeatedly for recent major earthquakes, such as the 1985 Mexico earthquake and the 1989 Loma Prieta earthquake.

As many recent studies have suggested, large earthquakes with a long fault length, such as those expected on the San Andreas fault, excite a highly significant amount of energy at periods longer than 1 s. In view of the high probability of large ($M > 7.5$) earthquakes on the San Andreas fault in the next 30 years[8], and possible large earthquakes on the blind faults beneath the Los Angeles basin[9], it is important to assess the long-period response of the Los Angeles basin quantitatively so that more comprehensive hazard mitigation measures can be taken.

FIG. 1 Arrival times of the shock waves excited by the space shuttle Columbia, recorded by seismic stations of the Southern California Seismic Network and The University of Southern California Los Angeles Basin Seismic Network. The numbers below the station codes are the arrival times (in seconds from an arbitrary reference time). Hyperbolas at 20 s intervals are fitted to the arrival-time data. The inset shows the stations PAS and SCS (at the University of Southern California) with respect to downtown Los Angeles. The vector V indicates the shuttle path. The arrival-time difference between PAS and SCS is 20.3 s.

FIG. 2 Comparison of the displacement records at PAS and SCS (for station locations, see Fig. 1) displayed on a common timescale. A high-pass-filtered record is shown above the displacement record for each station to indicate the arrival time of the shock wave. Note that at PAS the long-period P pulse arrives 12.5 s before the shock wave, whereas at SCS it is 3 s after the shock wave.

FIG. 3 Examples of N waves. The records represent ground-motion velocity in a frequency range of 1–10 Hz. The numbers to the right are the separations (in s) between the two pulses of an N wave.

Received 22 October 1990; accepted 8 January 1991.

Gene flow between African- and European-derived honey bee populations in Argentina

Walter S. Sheppard*, Thomas E. Rinderer†, Julio A. Mazzoli‡, J. Anthony Stelzer† & Hachiro Shimanuki*

* Bee Research Laboratory, USDA-ARS, Building 476, BARC-E, Beltsville, Maryland, 20705, USA
† Honey Bee Breeding, Genetics and Physiology Research Laboratory, USDA-ARS, 1157 Ben Hur Road, Baton Rouge, Louisiana, 70820, USA
‡ Catedra de Genética, Facultad de Agronomía, Universidad de Buenos Aires, 1417 Buenos Aires, Argentina

IN the Neotropics, introduced European honey bees (*Apis mellifera* L.)[1,2] have been largely supplanted by bees descended from an African race, *A. m. scutellata* Lepetier, which were introduced into Brazil in the 1950s. Recent restriction enzyme analyses indicate that mitochondrial DNA in some neotropical populations is almost entirely of African origin[3,4], and these data have been cited as evidence for asymmetrical gene flow between African- and European-derived populations[3,4]. Evaluation of the nature of hybridization in the Neotropics is, however, confounded by possible

Earthquake Mechanism

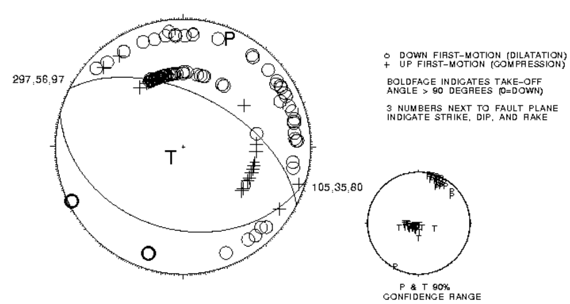

Earthquake Mechanism

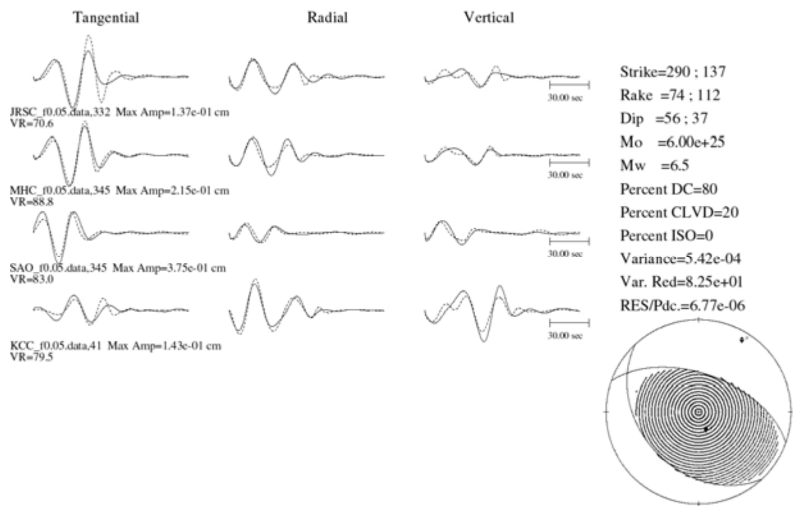

Earthquake Mechanism

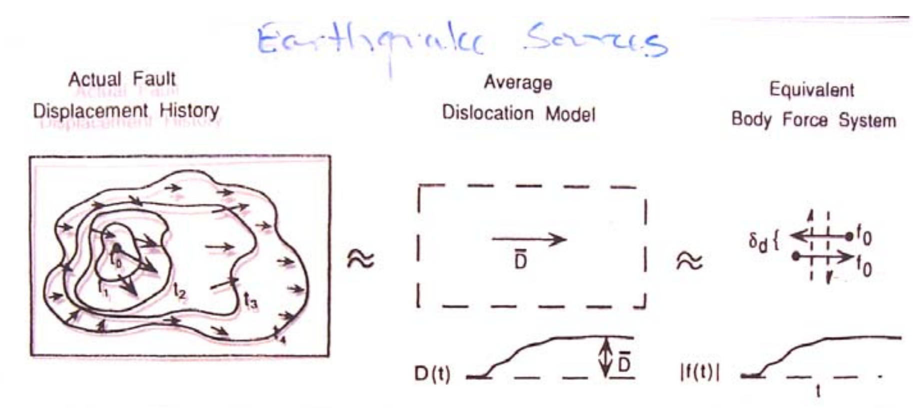

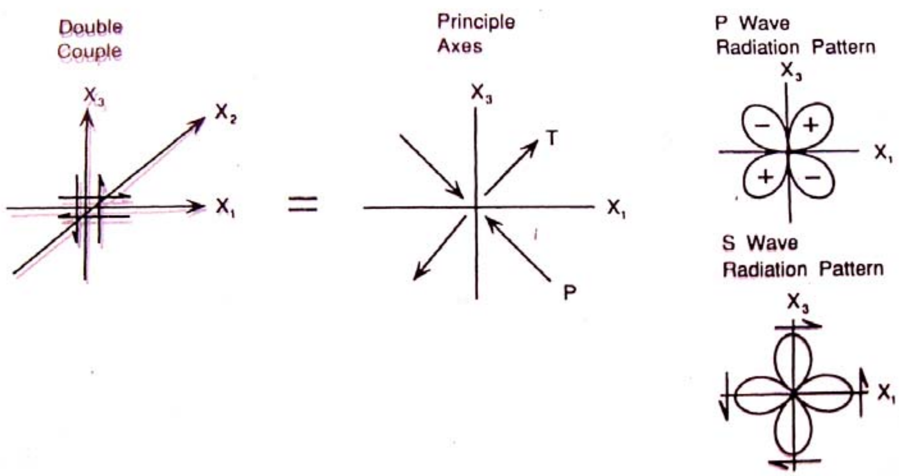
Double
Couple
X_3
X_2
X_1
Principle
Axes
X_3
T
X_1
P
P Wave
Radiation Pattern
X_3
–
+
X_1
+
–
S Wave
Radiation Pattern
X_3
X_1

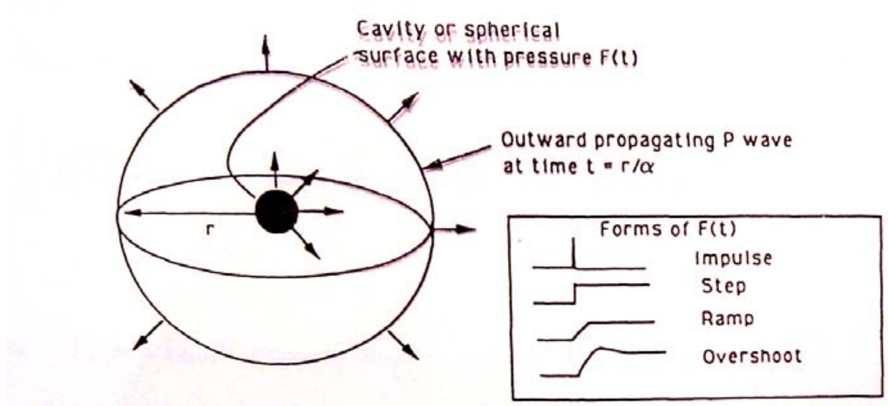
Cavity or spherical
surface with pressure F(t)
Outward propagating P wave
at time t = r/α
r
Forms of F(t)
Impulse
Step
Ramp
Overshoot

given $\frac{\partial^2 \phi}{\partial r^2} - \frac{1}{\alpha^2}\frac{\partial^2 \phi}{\partial t^2} = -4\pi F(t)\,\delta(r_0)$

Solutions $\phi(r,t) = \frac{-F(t - r/\alpha)}{r}$ are found

$$\tilde{\phi}(r,s) = -F(s)\,\frac{e^{-rs/\alpha}}{r}$$

The displacement field is then

$$\tilde{u} = \frac{\partial \phi}{\partial r} = F(s)\,\frac{e^{-rs/\alpha}}{r^2} + \left(sF(s)\right)\frac{e^{-rs/\alpha}}{r\alpha}$$

$$u(r,t) = \frac{F(t - r/\alpha)}{r^2} + \frac{\dot{F}(t - r/\alpha)}{\alpha r}$$

Near-field term

Far-field term

Near- & Far-field time histories

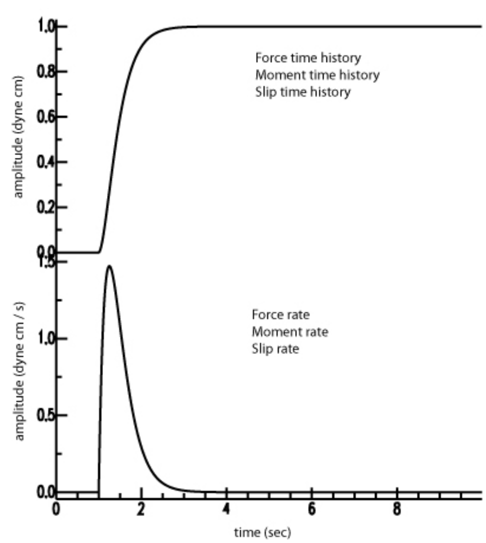

2004 Parkfield at PKD

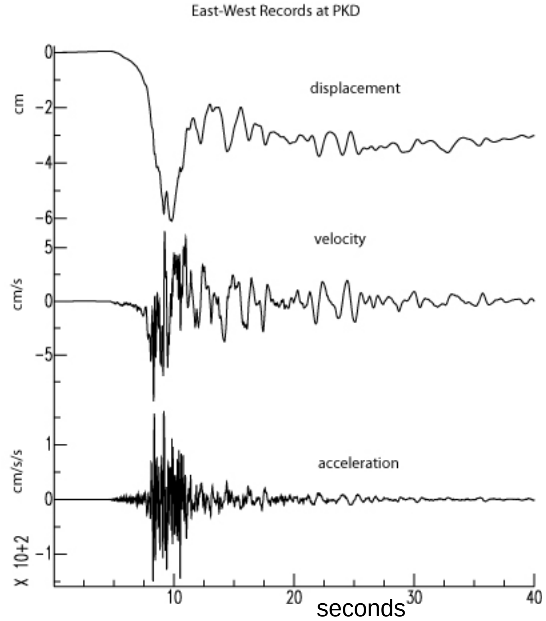

Elastodynamics

(1) $$\rho\ddot{u} = \rho\vec{f} + (\lambda + 2\mu)\nabla(\nabla\cdot\vec{u}) - \mu\nabla\times\nabla\times\vec{u}$$

Time dependent (varying) point force

$$\rho\vec{f} = F(t)\delta(r)\hat{a} = -F(t)\nabla^2\left(\frac{\hat{a}}{4\pi r}\right)$$

(2) $$= -F(t)\left\{\nabla\left(\nabla\cdot\left(\frac{\vec{a}}{4\pi r}\right)\right) - \nabla\times\nabla\times\left(\frac{\vec{a}}{4\pi r}\right)\right\}$$

seek solutions of the form

(3) $$u(t) = \nabla(\nabla\cdot\vec{A}_p) - \nabla\times\nabla\times\vec{A}_s$$

$\vec{A}_p$ & $\vec{A}_s$ are vector potential fields
where $\nabla\times\vec{A}_p = 0$ & $\nabla\cdot\vec{A}_s = 0$

seek solutions of the form

(3) $$u(t) = \nabla(\nabla\cdot\vec{A}_p) - \nabla\times\nabla\times\vec{A}_s$$

$\vec{A}_p$ & $\vec{A}_s$ are vector potential fields where $\nabla\times\vec{A}_p=0$ & $\nabla\cdot\vec{A}_s=0$

substituting (2) & (3) into (1) yields

$$\rho\nabla(\nabla\cdot\ddot{\vec{A}}_p) - \rho\nabla\times\nabla\times\ddot{\vec{A}}_s = -F(t)\nabla(\nabla\cdot(\tfrac{\vec{a}}{4\pi r})) + F(t)\nabla\times\nabla\times(\tfrac{\vec{a}}{4\pi r})$$

$$+ (\lambda+2\mu)(\nabla(\nabla\cdot\nabla(\nabla\cdot\vec{A}_p)) - \nabla(\nabla\cdot\nabla\times\nabla\times\vec{A}_s))$$

$$- \mu\nabla\times\nabla\times(\nabla(\nabla\cdot\vec{A}_p)) + \mu\nabla\times\nabla\times\nabla\times\nabla\times\vec{A}_s$$

Vector identities

$$\nabla\cdot(\nabla\times\vec{\Psi}) \equiv 0$$

$$\nabla\times(\nabla\phi) = 0$$

grouping terms results in two separable 2nd order wave equations

$$\left\{\rho\nabla(\nabla\cdot\ddot{\vec{A}}_p) + F(t)\nabla(\nabla\cdot(\tfrac{\vec{a}}{4\pi r})) - (\lambda+2\mu)\nabla(\nabla\cdot\nabla(\nabla\cdot\vec{A}_p))\right\}$$

$+$

$$\left\{-\rho\nabla\times\nabla\times\ddot{\vec{A}}_s - F(t)\nabla\times\nabla\times(\tfrac{\hat{a}}{4\pi r}) - \mu\nabla\times\nabla\times\nabla\times\nabla\times\vec{A}_s\right\} = \phi$$

$\vec{A}_p = A_p\hat{a}$ $\quad \vec{A}_s = A_s\hat{a}$ reducing to

scalar wave equations

$$\nabla^2 A_p - \frac{1}{\alpha^2}\ddot{A}_p = \frac{F(t)}{4\pi\alpha^2 r}$$

$$\nabla^2 A_s - \frac{1}{\beta^2}\ddot{A}_s = \frac{F(t)}{4\pi\beta^2 r}$$

$$\nabla^2 A_s - \frac{1}{\beta^2}\ddot{A}_s = \frac{F(t)}{4\pi\beta^2 r}$$

solutions are found by integrating general solutions over volume

$$A_p = \frac{1}{4\pi\alpha^2\rho}\iiint_V \frac{-F\left(\xi, t-\frac{|\vec{x}-\xi|}{\alpha}\right)}{|\vec{x}-\xi|}\,dV$$

and applying $\vec{u} = \nabla(\nabla\cdot\vec{A}_p) - \nabla\times\nabla\times\vec{A}_s$

yielding

Stokes solution

$$u_n(x,t) = \frac{1}{4\pi\rho}(3\gamma_n\gamma_p - \delta_{np})\frac{1}{r^3}\int_{r/\alpha}^{r/\beta}\tau F(t-\tau)\,d\tau + \frac{1}{4\pi\rho\alpha^2}\frac{1}{r}\gamma_n\gamma_p F(t-r/\alpha) - \frac{1}{4\pi\rho\beta^2}\frac{1}{r}(\gamma_n\gamma_p-\delta_{np})F\left(t-\frac{r}{\beta}\right)$$

$$\gamma_n = \frac{x_n}{r} = \frac{\partial r}{\partial x_n}$$

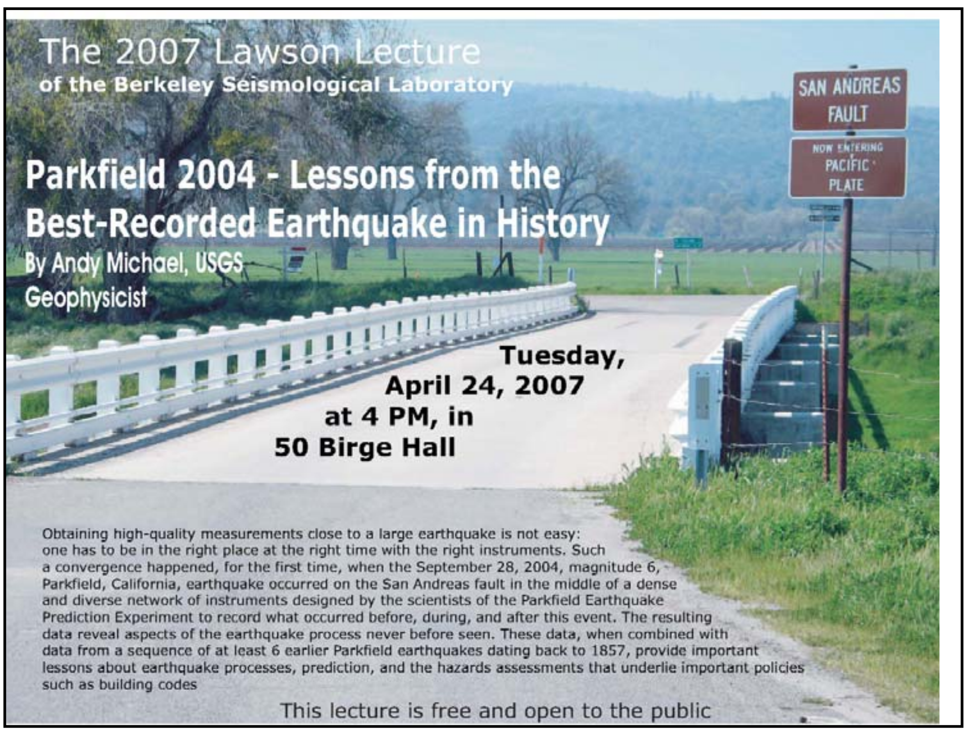

Berkeley Seismological Laboratory – Lawson Lecture

Single Force Radiation

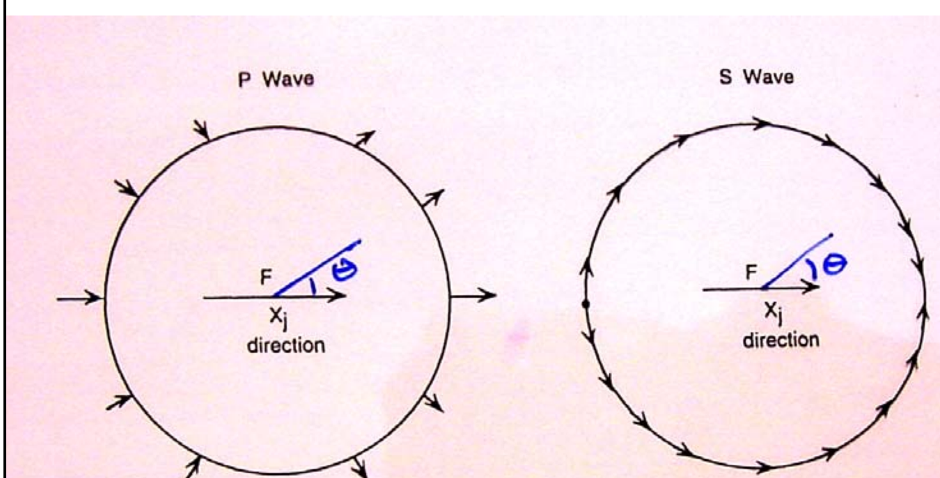

Far-field solutions for P-waves

direction of component — direction of $\vec{F}$

$$u_n(x,t) = \frac{1}{4\pi\rho\alpha^2}\frac{1}{r}\underbrace{\gamma_n\gamma_p}_{\text{radiation pattern}} F(t-r/\alpha)$$

and $\vec{F}$ in $p=1$ direction

considering the $\hat{x}_2$-plane

$$\vec{u}_1(\vec{x},t) = \frac{1}{4\pi\rho\alpha^2}\frac{1}{r}\gamma_1\gamma_3 F(t-r/\alpha)\hat{x}_3 + \frac{1}{4\pi\rho\alpha^2}\frac{1}{r}\gamma_1\gamma_1 F(t-r/\alpha)\hat{x}_1$$

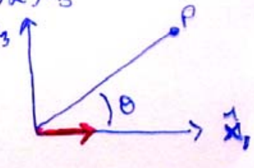

$\gamma_1 = \cos\theta$

$\gamma_3 = \cos(90-\theta) = \sin\theta$

$$\|u_1(x,t)\| = \frac{1}{4\pi\rho\alpha^2}\frac{1}{r}F(t-r/\alpha)\left[\cos^2\theta\sin^2\theta + \cos^4\theta\right]^{1/2}$$

$$= \frac{1}{4\pi\rho\alpha^2}\frac{1}{r}F(t-r/\alpha)\cos\theta$$

Far-field solution for S-waves considering $\hat{x}_2$-plane

$$u^s(x,t) = \left[\frac{1}{4\pi\rho\beta^2}\frac{1}{r}\right]\left((\gamma_1\gamma_1 - 1)\hat{x}_1 + \gamma_1\gamma_3\hat{x}_3\right)$$

since $\gamma_1\gamma_1 + \gamma_3\gamma_3 = 1$

$$\|u^s\| \propto \left[\sin^4\theta + \cos^2\theta\sin^2\theta\right]^{1/2} = \sin\theta$$

Direction Cosine Derivation of Force-Couple Radiation pattern

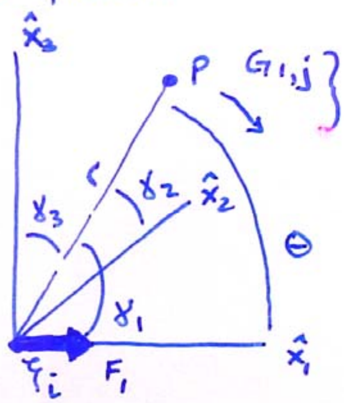

motion described by solution (Green's Function) due to $\vec{F}$

$$r = \left[(x_1-\xi_1)^2 + (x_2-\xi_2)^2 + (x_3-\xi_3)^2 \right]^{1/2}$$

$$r = \left[(x_1-\xi_1)^2 + (x_2-\xi_2)^2 + (x_3-\xi_3)^2 \right]^{1/2}$$

$$\frac{\partial r}{\partial x_1} = \frac{\frac{1}{2}\,2\,(x_1-\xi_1)}{r} = \frac{(x_1-\xi_1)}{r} = \cos\Theta = \gamma_1$$

therefore $\quad \dfrac{\partial r}{\partial x_i} = \gamma_i \qquad \dfrac{\partial r}{\partial \xi_i} = -\gamma_i$

it can also be shown that

$$\frac{\partial}{\partial x_i}\frac{1}{r} = \frac{-\gamma_i}{r^2}$$

$$\frac{\partial \gamma_i}{\partial x_j} = -\frac{1}{r}\left(\gamma_i \gamma_j - \delta_{ij} \right)$$

These derivatives allow determination of the response from a force-couple

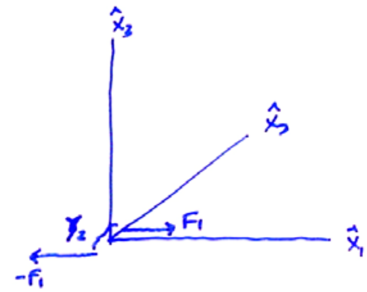

in the limit as $\xi_2 \to 0$ this is a spatial derivative

$$\therefore \quad F^{couple} = \frac{d}{d\xi_i} F_j^{SF}$$

consider a far-field P-wave

$$u_i^{SF} = \frac{1}{4\pi\rho\alpha^2} \gamma_i \gamma_j \frac{1}{r} F(t - r/\alpha)$$

derivatives of γ_i, γ_j & $1/r$ with respect to ξ_2 result in higher order terms of $1/r$ (i.e. $1/r^n$)

Ignoring these (the far-field approximation) gives

$$\frac{d}{d\xi_2} u_i^{SF} \approx \frac{1}{4\pi\rho\alpha^2} \gamma_i \gamma_j \frac{1}{r} \frac{d}{d\xi_2} F(t - r/\alpha)$$

$$= \frac{1}{4\pi\rho\alpha^2 r} \gamma_i \gamma_j \left(\dot{F}(t - r/\alpha) \frac{dr}{d\xi_2} \frac{1}{\alpha} \right)$$

$$= \frac{\gamma_i \gamma_j \gamma_2}{4\pi\rho\alpha^3 r} \dot{F}(t - r/\alpha)$$

For a force in the $\hat{x}_1$ direction

P-waves

$$u_i^c \approx \frac{\partial}{\partial \xi_2} u_i^{SF} = \frac{\gamma_i \gamma_1 \gamma_2}{4\pi\rho\alpha^3 r} \dot{F}(t - r/\alpha)$$

for S-waves

$$u_i^c = \frac{-(\gamma_1\gamma_i - \delta_{1i})\gamma_2}{4\pi\rho\beta^3 r} \dot{F}(t - r/\beta)$$

4.3 THE DOUBLE-COUPLE SOLUTION IN AN INFINITE HOMOGENEOUS MEDIUM 79

(4.28) is quite straightforward to apply to (4.27), using the two rules

$$\frac{\partial r}{\partial \xi_q} = -\gamma_q \quad \text{and} \quad \frac{\partial \gamma_j}{\partial \xi_q} = \frac{\gamma_j\gamma_q - \delta_{jq}}{r},$$

and the outcome is a displacement field (see (3.22)) having the nth component

$$\begin{aligned} M_{pq} * G_{np,q} = &\left(\frac{15\gamma_n\gamma_p\gamma_q - 3\gamma_n\delta_{pq} - 3\gamma_p\delta_{nq} - 3\gamma_q\delta_{np}}{4\pi\rho}\right)\frac{1}{r^4}\int_{r/\alpha}^{r/\beta} \tau M_{pq}(t-\tau)\,d\tau \\ &+ \left(\frac{6\gamma_n\gamma_p\gamma_q - \gamma_n\delta_{pq} - \gamma_p\delta_{nq} - \gamma_q\delta_{np}}{4\pi\rho\alpha^2}\right)\frac{1}{r^2}M_{pq}\left(t - \frac{r}{\alpha}\right) \\ &- \left(\frac{6\gamma_n\gamma_p\gamma_q - \gamma_n\delta_{pq} - \gamma_p\delta_{nq} - 2\gamma_q\delta_{np}}{4\pi\rho\beta^2}\right)\frac{1}{r^2}M_{pq}\left(t - \frac{r}{\beta}\right) \\ &+ \frac{\gamma_n\gamma_p\gamma_q}{4\pi\rho\alpha^3}\frac{1}{r}\dot{M}_{pq}\left(t - \frac{r}{\alpha}\right) \\ &- \left(\frac{\gamma_n\gamma_p - \delta_{np}}{4\pi\rho\beta^3}\right)\gamma_q\frac{1}{r}\dot{M}_{pq}\left(t - \frac{r}{\beta}\right). \end{aligned} \qquad (4.29)$$

From Aki & Richards, 1981

Single Couple Radiation Pattern

Considering the $\hat{x}_3$ plane for P-waves

$$u^c = \frac{\dot{M}(t - r/\alpha)}{4\pi\rho\alpha^3 r}\left[\gamma_1^2\gamma_2\,\hat{x}_1 + \gamma_1\gamma_2^2\,\hat{x}_2\right]$$

$$\gamma_1 = \cos\theta \qquad \gamma_2 = \sin\theta$$

&

$$\| u_i^c \| = \frac{\dot{M}(t - r/\alpha)}{4\pi\rho\alpha^3 r}\left[\cos^4\theta\sin^2\theta + \cos^2\theta\sin^4\theta\right]^{1/2}$$

$$\sin 2\theta = 2\sin\theta\cos\theta$$

$$= \frac{\dot{M}(t - r/\alpha)}{4\pi\rho\alpha^3 r}\left[\frac{1}{4}\sin^2 2\theta\left(\cos^2\theta + \sin^2\theta\right)\right]^{1/2}$$

$$= \frac{\dot{M}(t - r/\alpha)}{4\pi\rho\alpha^3 r}\left[\frac{1}{2}\sin 2\theta\right]$$

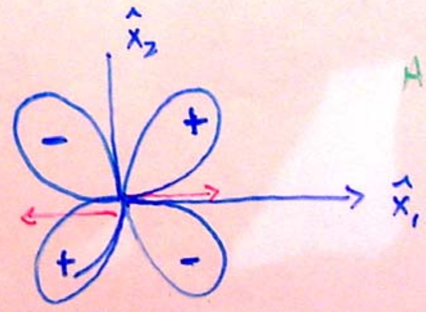

A 4-quadrant pattern

Now for $\hat{x}_3$ plane S-wave radiation

$$u_i^c = \frac{\dot{M}(t-r/\beta)}{4\pi\rho\beta^3 r}\left[(1-\gamma_1^2)\gamma_2\hat{x}_1 - \gamma_1\gamma_2^2\hat{x}_2\right]$$

since $\gamma_1^2+\gamma_2^2=1$

$\gamma_2^2 = 1-\gamma_1^2$

&

$$\|u_i^c\| = \frac{\dot{M}(t-r/\beta)}{4\pi\rho\beta^3 r}\left[\gamma_2^6 + \gamma_1^2\gamma_2^4\right]^{1/2}$$

$$= \frac{\dot{M}(t-r/\beta)}{4\pi\rho\beta^3 r}\left[\sin^2\theta\right]$$

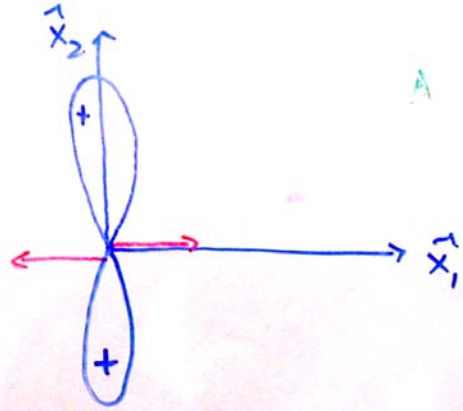

Double Couples

Simply the sum of two couples

$\hat{x}_3$ -plane

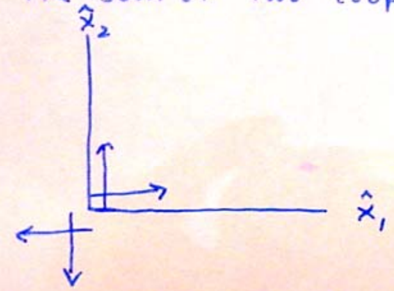

P waves

$$u_i^{DC} = \frac{2\gamma_1\gamma_2\gamma_n \dot{M}(t-r/\alpha)}{4\pi\rho\alpha^3 r}\hat{x}_i$$

same 4-lobed pattern due to a single-couple

S waves

$$u_i^{DC} = \frac{(\delta_{1i}-\gamma_1\gamma_i)\gamma_2\dot{M}(t-r/\beta)}{4\pi\rho\beta^3 r}\hat{x}_i + \frac{(\delta_{2i}-\gamma_2\gamma_i)\gamma_1\dot{M}(t-r/\beta)}{4\pi\rho\beta^3 r}\hat{x}_i$$

$$= \left[\frac{\dot{M}(t-r/\beta)}{4\pi\rho\beta^3 r}\right]\left[((1-\gamma_1^2)\gamma_2 - \gamma_1^2\gamma_2)\hat{x}_1 + ((1-\gamma_2^2)\gamma_1 - \gamma_1\gamma_2^2)\hat{x}_2\right]$$

$$= \left[\frac{\dot{M}(t-r/\beta)}{4\pi\rho\beta^3 r}\right]\left[(\gamma_2^3 - \gamma_1^2\gamma_2)\hat{x}_1 + (\gamma_1^3 - \gamma_1\gamma_2^2)\hat{x}_2\right]$$

$$= \left[\frac{\dot{M}(t-r/\beta)}{4\pi\rho\beta^3 r}\right]\left[\gamma_2(\gamma_2^2-\gamma_1^2)\hat{x}_1 + \gamma_1(\gamma_1^2-\gamma_2^2)\hat{x}_2\right]$$

since $\gamma_1 = \cos\theta$ & $\gamma_2 = \sin\theta$

and $\gamma_1^2 - \gamma_2^2 = \cos^2\theta - \sin^2\theta = \cos 2\theta$

$$\| u^{dc} \| = \frac{\dot{m}(t - r/\beta)}{4\pi\rho\beta^3 r} \cos 2\theta$$

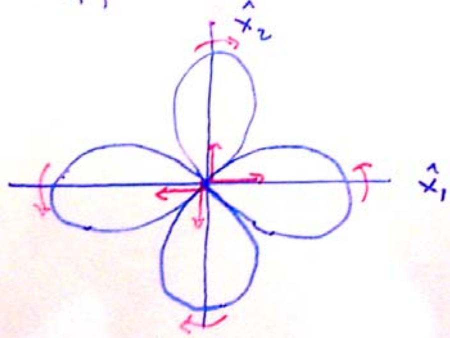

(4.28) is quite straightforward to apply to (4.27), using the two rules

$$\frac{\partial r}{\partial \xi_q} = -\gamma_q \quad \text{and} \quad \frac{\partial \gamma_j}{\partial \xi_q} = \frac{\gamma_j \gamma_q - \delta_{jq}}{r},$$

and the outcome is a displacement field (see (3.22)) having the nth component

$$\begin{aligned} M_{pq} * G_{np,q} = &\left(\frac{15\gamma_n\gamma_p\gamma_q - 3\gamma_n\delta_{pq} - 3\gamma_p\delta_{nq} - 3\gamma_q\delta_{np}}{4\pi\rho} \right) \frac{1}{r^4} \int_{r/\alpha}^{r/\beta} \tau M_{pq}(t - \tau)\, d\tau \\ &+ \left(\frac{6\gamma_n\gamma_p\gamma_q - \gamma_n\delta_{pq} - \gamma_p\delta_{nq} - \gamma_q\delta_{np}}{4\pi\rho\alpha^2} \right) \frac{1}{r^2} M_{pq}\left(t - \frac{r}{\alpha}\right) \\ &- \left(\frac{6\gamma_n\gamma_p\gamma_q - \gamma_n\delta_{pq} - \gamma_p\delta_{nq} - 2\gamma_q\delta_{np}}{4\pi\rho\beta^2} \right) \frac{1}{r^2} M_{pq}\left(t - \frac{r}{\beta}\right) \\ &+ \frac{\gamma_n\gamma_p\gamma_q}{4\pi\rho\alpha^3} \frac{1}{r} \dot{M}_{pq}\left(t - \frac{r}{\alpha}\right) \\ &- \left(\frac{\gamma_n\gamma_p - \delta_{np}}{4\pi\rho\beta^3} \right) \gamma_q \frac{1}{r} \dot{M}_{pq}\left(t - \frac{r}{\beta}\right). \end{aligned} \qquad (4.29)$$

From Aki & Richards, 1981

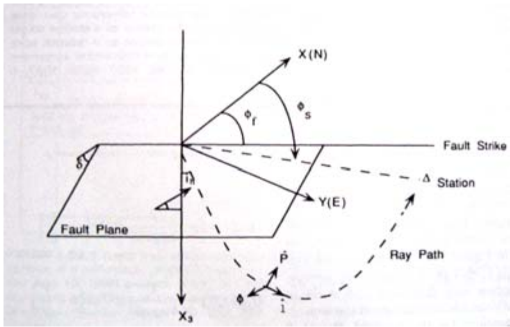

$$
\begin{aligned}
R^P = {} & \cos\lambda \sin\delta \sin^2 i_h \sin 2\phi \\
& - \cos\lambda \cos\delta \sin 2i_h \cos\phi \\
& + \sin\lambda \sin 2\delta (\cos^2 i_h - \sin^2 i_h \sin^2\phi) \\
& + \sin\lambda \cos 2\delta \sin 2i_h \sin\phi \\
R^{SV} = {} & \sin\lambda \cos 2\delta \cos 2i_h \sin\phi \\
& - \cos\lambda \cos\delta \cos 2i_h \cos\phi \\
& + \tfrac{1}{2} \cos\lambda \sin\delta \sin 2i_h \sin 2\phi \\
& - \tfrac{1}{2} \sin\lambda \sin 2\delta \sin 2i_h (1 + \sin^2\phi) \\
R^{SH} = {} & \cos\lambda \cos\delta \cos i_h \sin\phi \\
& + \cos\lambda \sin\delta \sin i_h \cos 2\phi \\
& + \sin\lambda \cos 2\delta \cos i_h \cos\phi \\
& - \tfrac{1}{2} \sin\lambda \sin 2\delta \sin i_h \sin 2\phi,
\end{aligned}
\tag{8.65}
$$

$$U_P(r,t) = \frac{1}{4\pi\rho r\alpha^3} R^P \dot{M}\left(t - \frac{r}{\alpha}\right)$$

$$U_{SV}(r,t) = \frac{1}{4\pi\rho r\beta^3} R^{SV} \dot{M}\left(t - \frac{r}{\beta}\right)$$

$$U_{SH}(r,t) = \frac{1}{4\pi\rho r\beta^3} R^{SH} \dot{M}\left(t - \frac{r}{\beta}\right)$$

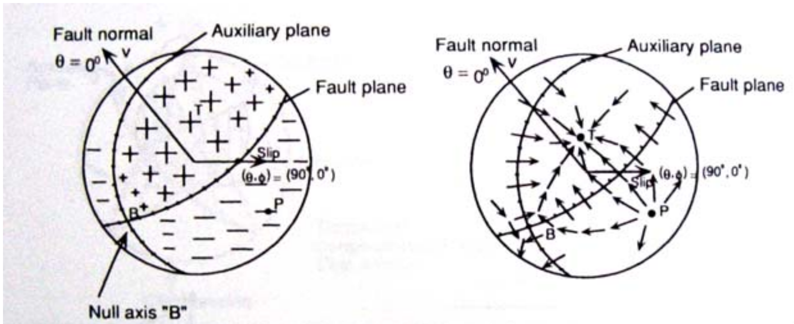

FIGURE 8.27 Focal mechanisms for an oblique-slip event showing *P*-wave polarities and relative amplitudes (left) and *S*-wave polarizations and amplitudes (right). Plus signs (+) indicate compressions. The fault and auxiliary planes are shown as well as projections of the *P*, *T*, and *B* axes. (Modified from Aki and Richards, 1980. Copyright ©1980 by W. H. Freeman and Co. Reprinted with permission.)

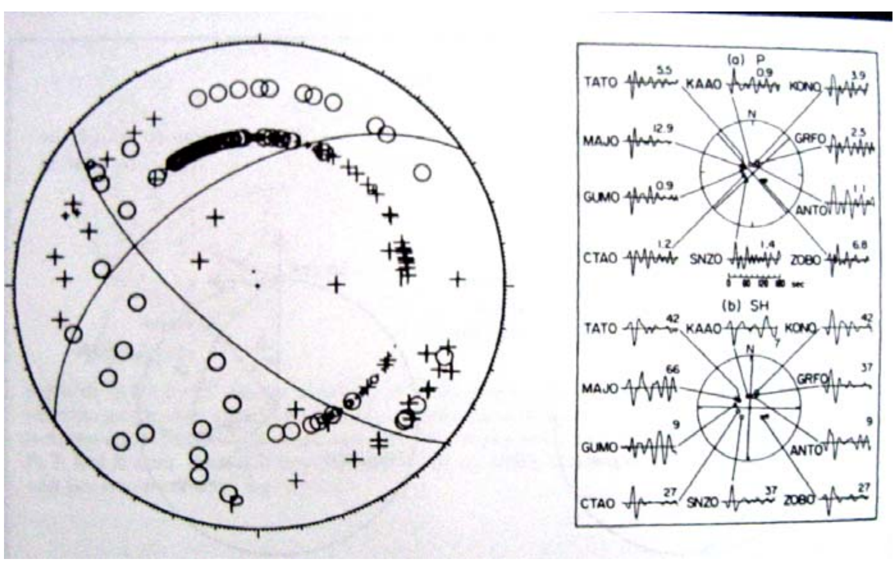

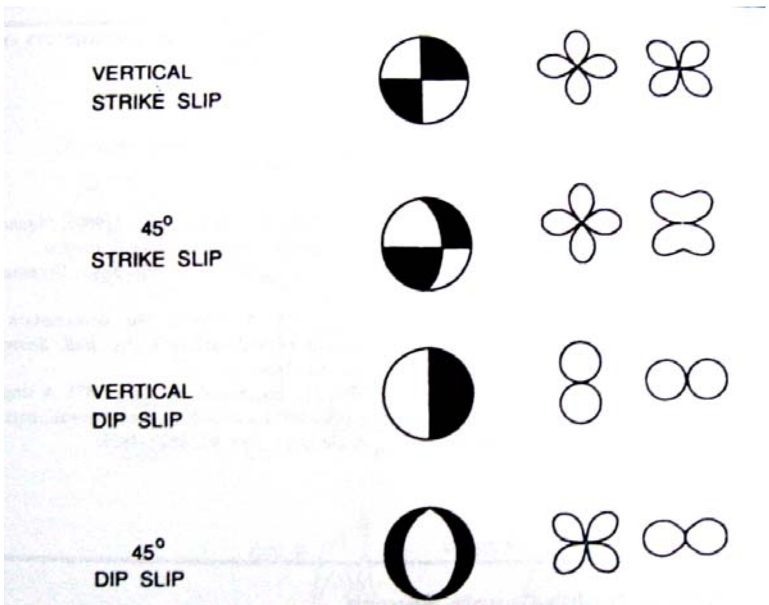
VERTICAL
STRIKE SLIP
45°
STRIKE SLIP
VERTICAL
DIP SLIP
45°
DIP SLIP

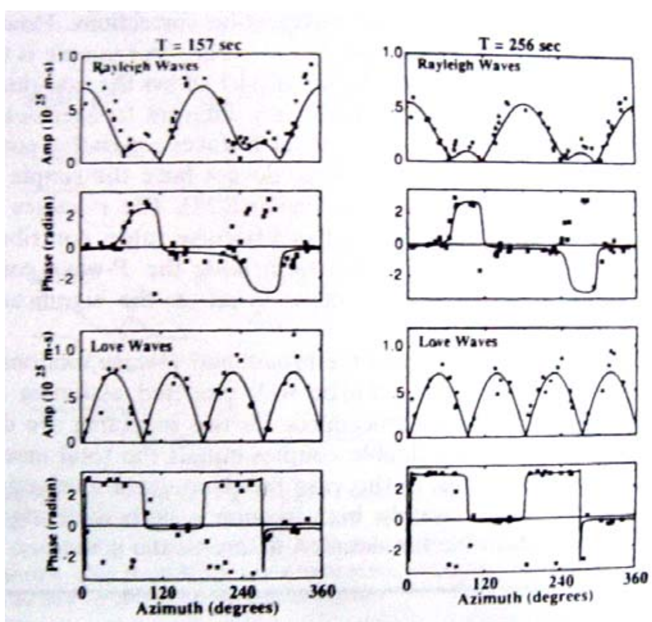
T = 157 sec
T = 256 sec
Rayleigh Waves
Love Waves
Amp (10 25 m-s)
Phase (radian)
Azimuth (degrees)

$$U_P(r,t) = \frac{1}{4\pi\rho r\alpha^3} R^P \dot{M}\left(t - \frac{r}{\alpha}\right)$$

$$U_{SV}(r,t) = \frac{1}{4\pi\rho r\beta^3} R^{SV} \dot{M}\left(t - \frac{r}{\beta}\right)$$

$$U_{SH}(r,t) = \frac{1}{4\pi\rho r\beta^3} R^{SH} \dot{M}\left(t - \frac{r}{\beta}\right)$$

(4.28) is quite straightforward to apply to (4.27), using the two rules

$$\frac{\partial r}{\partial \xi_q} = -\gamma_q \quad \text{and} \quad \frac{\partial \gamma_j}{\partial \xi_q} = \frac{\gamma_j \gamma_q - \delta_{jq}}{r}.$$

and the outcome is a displacement field (see (3.22)) having the nth component

$$\begin{aligned} M_{pq} * G_{np,q} = {} & \left(\frac{15\gamma_n\gamma_p\gamma_q - 3\gamma_n\delta_{pq} - 3\gamma_p\delta_{nq} - 3\gamma_q\delta_{np}}{4\pi\rho}\right)\frac{1}{r^4}\int_{r/\alpha}^{r/\beta} \tau M_{pq}(t-\tau)\,d\tau \\ & + \left(\frac{6\gamma_n\gamma_p\gamma_q - \gamma_n\delta_{pq} - \gamma_p\delta_{nq} - \gamma_q\delta_{np}}{4\pi\rho\alpha^2}\right)\frac{1}{r^2} M_{pq}\left(t - \frac{r}{\alpha}\right) \\ & - \left(\frac{6\gamma_n\gamma_p\gamma_q - \gamma_n\delta_{pq} - \gamma_p\delta_{nq} - 2\gamma_q\delta_{np}}{4\pi\rho\beta^2}\right)\frac{1}{r^2} M_{pq}\left(t - \frac{r}{\beta}\right) \\ & + \frac{\gamma_n\gamma_p\gamma_q}{4\pi\rho\alpha^3}\frac{1}{r}\dot{M}_{pq}\left(t - \frac{r}{\alpha}\right) \\ & - \left(\frac{\gamma_n\gamma_p - \delta_{np}}{4\pi\rho\beta^3}\right)\gamma_q\frac{1}{r}\dot{M}_{pq}\left(t - \frac{r}{\beta}\right). \end{aligned} \quad (4.29)$$

$$\mathbf{u}(\mathbf{x},t) = \frac{1}{4\pi\rho}\mathbf{A}^N \frac{1}{r^4}\int_{r/\alpha}^{r/\beta} \tau M_0(t-\tau)\,d\tau$$

$$+ \frac{1}{4\pi\rho\alpha^2}\mathbf{A}^{IP}\frac{1}{r^2}M_0\left(t-\frac{r}{\alpha}\right) + \frac{1}{4\pi\rho\beta^2}\mathbf{A}^{IS}\frac{1}{r^2}M_0\left(t-\frac{r}{\beta}\right) \quad (4.32)$$

$$+ \frac{1}{4\pi\rho\alpha^3}\mathbf{A}^{FP}\frac{1}{r}\dot{M}_0\left(t-\frac{r}{\alpha}\right) + \frac{1}{4\pi\rho\beta^3}\mathbf{A}^{FS}\frac{1}{r}\dot{M}_0\left(t-\frac{r}{\beta}\right).$$

in which the near-field, the intermediate-field P and S, and the far-field P and S have radiation patterns given, respectively, by

$$\begin{aligned}
\mathbf{A}^N &= 9\sin 2\theta\cos\phi\,\hat{\mathbf{r}} - 6(\cos 2\theta\cos\phi\,\hat{\boldsymbol{\theta}} - \cos\theta\sin\phi\,\hat{\boldsymbol{\phi}})\\
\mathbf{A}^{IP} &= 4\sin 2\theta\cos\phi\,\hat{\mathbf{r}} - 2(\cos 2\theta\cos\phi\,\hat{\boldsymbol{\theta}} - \cos\theta\sin\phi\,\hat{\boldsymbol{\phi}})\\
\mathbf{A}^{IS} &= -3\sin 2\theta\cos\phi\,\hat{\mathbf{r}} + 3(\cos 2\theta\cos\phi\,\hat{\boldsymbol{\theta}} - \cos\theta\sin\phi\,\hat{\boldsymbol{\phi}}) \qquad (4.33)\\
\mathbf{A}^{FP} &= \sin 2\theta\cos\phi\,\hat{\mathbf{r}}\\
\mathbf{A}^{FS} &= \cos 2\theta\cos\phi\,\hat{\boldsymbol{\theta}} - \cos\theta\sin\phi\,\hat{\boldsymbol{\phi}}.
\end{aligned}$$

These radiation patterns explicitly display a radial component, proportional to $\sin 2\theta \cos\phi\,\hat{\mathbf{r}}$, and a transverse component, proportional to $(\cos 2\theta\cos\phi\,\hat{\boldsymbol{\theta}} - \cos\theta\sin\phi\,\hat{\boldsymbol{\phi}})$. The important property brought out by (4.33) is that these are the only two radiation patterns needed to obtain a complete picture of all the different terms in the displacement field radiated from a shear dislocation (double couple). Figure 4.5 shows the way in which

Some Examples: Event Location

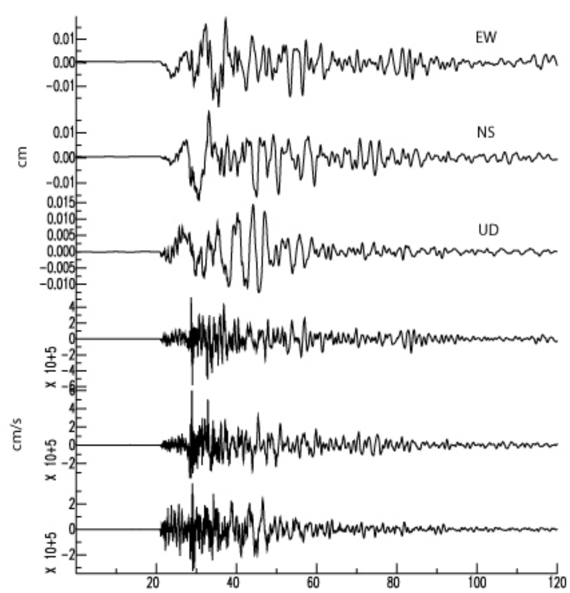

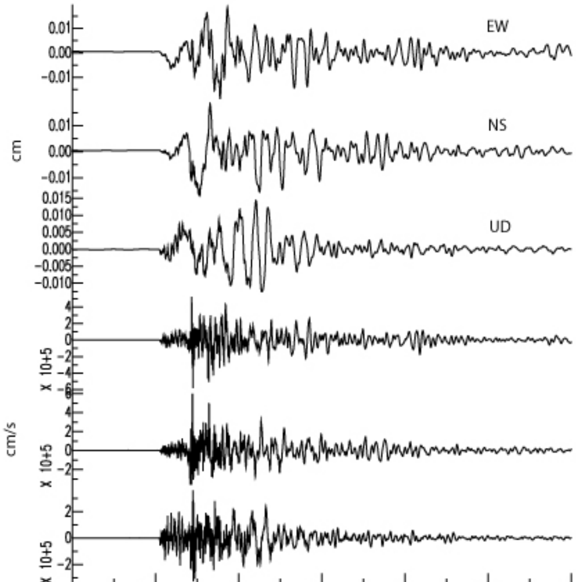

Ts-Tp=7.6 sec

$$T_s - T_p = \frac{x}{\beta} - \frac{x}{\alpha} = \frac{x}{\alpha}\left(\sqrt{3}-1\right)$$

$$x = \frac{\alpha\left(T_s - T_p\right)}{\sqrt{3}-1} = \frac{6}{0.732}\left(T_s - T_p\right) \approx 8 \cdot \left(T_s - T_p\right)$$

x=8*7.6=61 km

How can we determine the azimuth??

What can we estimate from these waveforms?

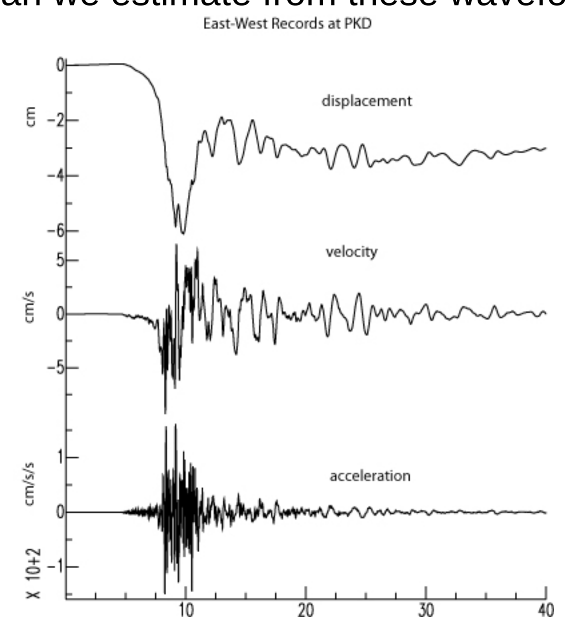

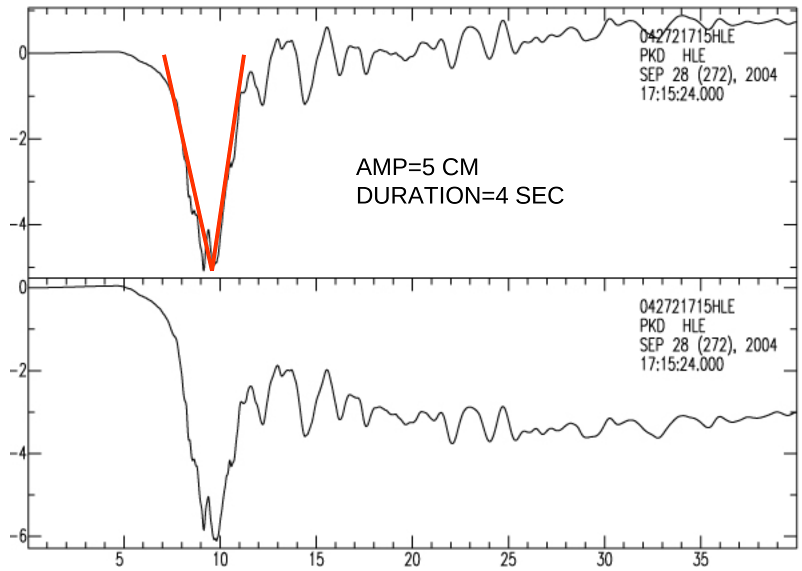

$$u = \frac{R \cdot \dot{M}}{4\pi\rho r \beta^3}$$

$$\int u\,dt = \frac{1}{2}A\tau = \frac{R \cdot M_0}{4\pi\rho r \beta^3}$$

$$M_0 = \frac{\left(2\pi\rho r \beta^3\right)A\tau}{R} = 2*3.14*2.67*8\cdot 10^5*(3.5\cdot 10^5)^3*5*4$$

$$= 1.14\cdot 10^{25}\ dyne\ cm$$

$$Mw = 6.0$$

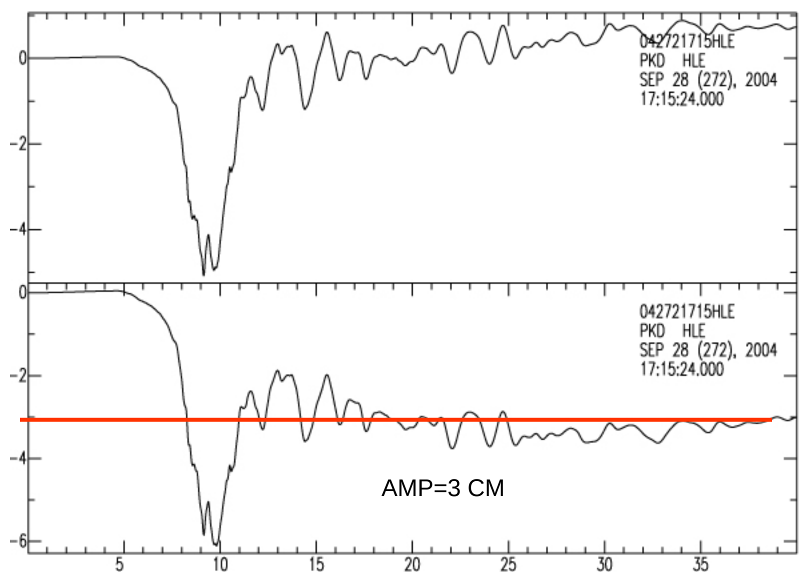

$$u_{static} = \frac{3 \cdot R \cdot M_0}{4\pi\rho r^2 \beta^2}$$

$$M_0 = \frac{\left(4\pi\rho r^2 \beta^2\right) u_{static}}{3R} = \frac{4}{3} * 3.14 * 2.67 * (8 \cdot 10^5)^2 * (3.5 \cdot 10^5)^2 * 3$$

$$= 2.63 \cdot 10^{24}\ dyne\ cm$$

$$Mw = 5.6$$

Interpretation of FM Mechanisms